Synoptic Flow and Density Observations near an Arctic Shelf Break

ANDREAS MÜNCHOW

Institute of Marine and Coastal Sciences, Rutgers University, New Brunswick, New Jersey

EDDY C. CARMACK

Institute of Ocean Sciences, Sidney, British Columbia, Canada

(Manuscript received 8 July 1996, in final form 14 January 1997)

ABSTRACT

Analyses of data from three shipborne surveys describe the quasi-synoptic density and velocity fields near Barrow Canyon, Alaska. The canyon parallels the northwestern coast of Alaska and contains three different water masses. These are 1) warm and fresh Alaskan coastal waters that originate from the Bering Strait; 2) cold and moderately salty waters that originate from the Chukchi shelf; and 3) warm and salty waters that originate from the Atlantic layer of the Arctic Ocean. A halocline separates the Chukchi shelf and Atlantic layer waters. The halocline slopes upward into the canyon where it is then twisted to slope across the wide canyon. An intensification of the Beaufort gyre near the shelf break just seaward of Barrow Canyon raises the halocline more than 100 m toward the surface. Locally upwelling favorable winds raise the Arctic halocline, which thus is ventilated within Barrow Canyon adjacent to the coast. In the absence of winds the halocline slopes across-canyon in the thermal wind sense due to a northward flowing coastal current.

Velocity measurements from a towed acoustic Doppler current profiler reveal a northward flowing jet that transports about 0.3 Sv (Sv $\equiv 10^6$ kg m^{-3}) of Bering Sea summer water into the Arctic Ocean at speeds that exceed 0.7 m s^{-1}. Total northward transports through the canyon exceed 1.0 Sv. The warm waters of this coastal current supply more than 100 W m^{-2} of heat to the atmosphere. The jet separates both from the bottom and from the coast. Hence, a laterally and vertically sheared jet forms, which breaks into three branches at about 71.8°N latitude.

1. Introduction

A steric height difference of about 0.5 m (relative to a reference level of 1000 m) between the Pacific and Arctic Oceans drives a mean northward flow across the Bering and Chukchi shelves (Stigebrandt 1984). The observed annual mean transport through the 50-m-deep Bering Strait is about 0.8 Sv (Sv $\equiv 10^6$ m^3 s^{-1}) (Coachman and Aagaard 1988), which agrees well with the transports predicted by a barotropic model (Overland and Roach 1987). In order to reach the Arctic Ocean, however, the flow through Bering Strait must cross the wide and shallow Chukchi shelf. An important part of this flow is the northward setting coastal current that flows along the west coast of Alaska from Bering Strait to Barrow Canyon (Paquette and Bourke 1974). Here we discuss data from shipborne hydrographic (CTD) and acoustic Doppler current profiler (ADCP) surveys to describe the structure and variability of this flow as it encounters the shelf break over Barrow Canyon.

In the summer and early fall warm and fresh Alaskan coastal waters from the eastern Bering Sea generally arrive at Point Barrow and pass through Barrow Canyon into the Arctic Ocean (Paquette and Bourke 1974; Ahlnäs and Garrison 1984; Aagaard and Roach 1990). Aagaard (1984) and Hufford (1973) use the pronounced temperature signal of these waters to infer an alongshore current over the slope of the Beaufort Sea. Current fluctuations correlate with both the atmospheric pressure difference along the western coast of Alaska and the local alongshore winds (Mountain et al. 1976; Coachman and Aagaard 1988). This generally strong correlation breaks down, however, when buoyant waters arrive from the south in the summer and fall. We argue below that during this season buoyancy-forced motions contribute to the dynamics of the eastern Chukchi Sea and Barrow Canyon.

The presence of Bering Strait waters in the Arctic interior was noted by Coachman and Barnes (1961), who searched early hydrographic data from the Arctic basins and found a persistent temperature maximum at about 70-m depth throughout much of the eastern Canada Basin. Tracing similar water masses along the continental slope of the Beaufort Sea, Hufford (1973, 1974), Mountain et al. (1976), and Aagaard (1984) postulate

Corresponding author address: Dr. Andreas Münchow, Institute of Marine and Coastal Sciences, Rutgers University, P.O. Box 231, New Brunswick, NJ 08903.

that the subsurface temperature maximum over the slope of the Beaufort Sea is due to warm waters from Bering Strait entering through Barrow Canyon. Property distributions (Hufford 1974) and direct velocity measurements (Aagaard 1989) indicate a subsurface eastward flow against the local winds over the slope of the Beaufort Sea. This current bears strong similarities to the subsurface slope currents found off California, Ireland, and northwest Africa (Huthnance 1992). The dynamics and spatial distribution of slope currents in the Arctic Ocean are largely unknown even though Aagaard (1989) postulates that they constitute the major circulation feature of this ocean.

Submarine canyons bordering the Arctic Ocean facilitate the exchange of mass, heat, and momentum between the wide continental shelves and the deep basins. Their width often exceeds the internal deformation radius, and geostrophically balanced baroclinic flows in the opposite direction are theoretically possible on opposing sides of the canyon (Klinck 1989). Little is known, however, on the spatial distribution of currents in wide Arctic canyons. For example, recirculation and enhanced upwelling may occur in any or all of the wide Arctic canyons, for example, the Santa Anna (at 75°E), Kolyma (at 160°E), Herald (at 170°W), Barrow (at 155°W), and Mackenzie (at 140°W) Canyons. Hanzlick and Aagaard (1980) interpret hydrographic data from the Santa Anna Canyon off Siberia in terms of a recirculating flow within this canyon. Only Mountain et al. (1976) and Aagaard and Roach (1990) report direct observations from one and two current meter moorings, respectively, deployed in Barrow Canyon off Alaska. Their data describe a rectilinear, seasonally averaged flow of about 0.2 m s^{-1} and peak currents that exceed 0.8 m s^{-1}. These are exceptionally large currents when compared to the generally quiescent interior Arctic Ocean where measured flows rarely exceed 0.05 m s^{-1} (Aagaard 1989); however, no spatial flow field observations are available from any Arctic canyon. This study of Barrow Canyon provides the first synoptic observations of both the spatial velocity and density fields of a wide Arctic canyon.

Canyon throughflows may also constitute a source of mesoscale variability in the ocean interior. Aagaard and Carmack (1994) suggest that such motions are a key mechanism of shelf–basin exchange in the Arctic Ocean. Newton et al. (1974), Manley and Hunkins (1985), and D'Asaro (1988a) all describe isolated submesoscale eddies as an ubiquitous feature of the interior circulation of the Canada Basin. Hart and Killworth (1976) employed linear stability analysis to show that these eddies could not have formed within the interior ocean. Their analysis and water mass characteristics of the observed eddies implicate a source region near a continental shelf. Using mass flux requirements, D'Asaro (1988b) argued that such eddies form in the vicinity of Barrow Canyon at a rate of about twice per day. Nevertheless, observations to verify this estimate are lacking, and it is thus unclear where, when, and how the submesocale eddies of the Arctic Ocean form. D'Asaro (1988b) proposed strong currents and lateral current shears in Barrow Canyon as key elements for the generation of submesoscale vortices. Commenting on the similarity of these eddies with those found near the Mediterranean outflow, he hypothesized lateral friction to shear a strong boundary current that subsequently separates from the coast. Stern and Whitehead (1990) simulated the separation of a barotropic jet from a sharp boundary in a rotating system both analytically and with a rotating tank. They find that separation occurs only for certain upstream lateral velocity profiles in conjunction with a critical corner angle. Klinger (1994) generalized the laboratory experiments by allowing a sloping bottom as well as density stratification to enter the problem. His results, however, are less clear as the parameter range has increased vastly and no unifying interpretation was given.

This study provides a first synoptic description of the spatially variable flow and density field of Barrow Canyon. Our study focuses on the northern terminus of the northward shelf flow that extends from Bering Strait in the south to Barrow Canyon in the north. Section 2 details our study area and instrumentation consisting of a towed ADCP and standard hydrographic profiling sensors (CTD). In section 3 we describe the water masses and their spatial distribution in and near the canyon. Across-shelf exchange processes involve both the along- and across-canyon density structures. Section 4 discusses the synoptic circulation over and near the canyon and shows how Bering Sea waters exit the Chukchi shelf through Barrow Canyon. Section 5 synthesizes hydrographic and flow field observations, presents quantitative estimates of property fluxes through the canyon, and speculates on the dynamics of the flow.

2. Study area and data sources

Barrow Canyon connects the Chukchi and Beaufort shelves with the deep Canada Basin of the Arctic Ocean. The canyon constitutes a deep, wide, and long intersection across the Chukchi shelf that runs almost parallel to the coastline of northwestern Alaska and intersects the east–west extending continental slope of the Arctic Ocean near Point Barrow, Alaska (Fig. 1). Here the coastline changes its orientation by 90° and the canyon separates the Chukchi shelf to the west of Point Barrow from the Beaufort shelf to the east. The two adjacent shelves differ substantially. The Chukchi shelf is shallow ($<$50 m), wide ($>$200 km), and gently sloping. In contrast, the Beaufort shelf is deeper ($<$100 m), narrower ($<$40 km), and more steeply sloping. Barrow Canyon thus separates three different oceanographic regimes: the Chukchi shelf, the Beaufort shelf, and the deep Canada Basin. Barrow Canyon is an area of temporally variable convergence and divergence since each of these regimes responds differently to atmospheric forcing. Anecdotal evidence collected by experienced

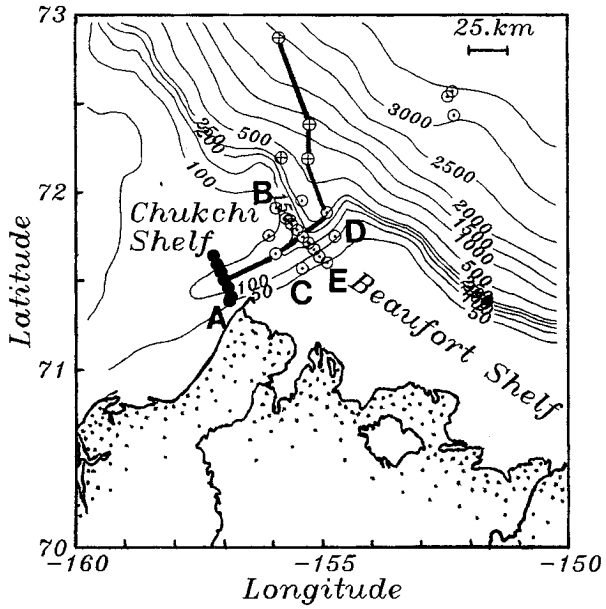

FIG. 1. Map of the study area at the northwestern tip of Alaska. Contours represent bottom topography in meters. The contour intervals are 50 and 500 m for depth interval (50, 500) m and (500, 3500) m, respectively. Also shown are CTD station locations that were occupied in August and September of 1993 by the USCGC *Polar Star* (circles with "+") and the CCGS *Henry Larsen* (filled circles for survey on 9 September 1993; circle with "•" for survey on 24–25 September 1993), respectively. Letters A through E label ADCP sections; E is a repeat of B. The thick solid line indicates the transect line of Figs. 3 and 5.

captains of icebreakers supports this notion as they often report of unpredictable, complex, rapidly evolving, and permanently changing patterns of ice and fog near Point Barrow. Accordingly, we expect and indeed find large spatial property gradients and large exchanges of mass, heat, and buoyancy near the canyon.

From aboard the Class 4 Icebreaker CCGS *Henry Larsen* we collected velocity and CTD data across and along the shelf break and Barrow Canyon. Relevant topographic slopes are 0.025, 0.013, and 0.002 across the shelf break north of Barrow, across the canyon east of Barrow, and up the talweg of the canyon south of Barrow, respectively (Fig. 1). Our most extensive survey took place on 24–25 September 1993 when we collected data along a circular ship track and along two acrosscanyon transects at 72°N latitude (Fig. 1). Our survey constituted the first application of a shipborne ADCP in the western Arctic Ocean. ADCPs have been deployed extensively at midlatitudes in studies of both the coastal (Münchow et al. 1992; Candela et al. 1992; Geyer and Signell 1990) and the deep ocean (Chereskin et al. 1989; Pollard and Regier 1992). ADCP applications in the Barents and Greenland Seas have been reported by Gawarkiewicz and Pluedderman (1995) and Johnson and Niebauer (1995), respectively. In contrast to the above applications, which use a vessel-mounted ADCP, we employ an ADCP system that is towed beside the bow of the ship at a fixed depth 14 m below the surface or about 7 m below the hull of the icebreaker.

The tow system was developed at the Scripps Institution of Oceanography and was tested extensively prior to its first operational application in the Arctic Ocean. The hydrodynamically shaped tow body housed a downward looking 153-kHz narrowband ADCP of RDI. Our subsurface tow does not entrain air bubbles, which frequently degrade the data quality of vessel mounted ADCP data (New 1992). The tow body constitutes a stable platform for an ADCP because its motions are largely decoupled from ship motions due to surface gravity waves. Münchow et al. (1995) report standard deviations of pitch, roll, and altitude of the tow system of about 0.6°, 0.4°, and 0.2 m, respectively. These values apply to tows at moderate ship speeds (6–8 kt), sea states (waves 1.5 m high), and winds (5–10 m s^{-1}). The conditions off Barrow Canyon in September 1993 were indeed moderate. Throughout all surveys we collected velocity data in 8-m vertical bins with 4 pings per ensemble every 10 seconds. These raw data were screened thoroughly to insure data quality before a 10-min average was formed (Münchow et al. 1995). The ADCP tracked the bottom at all times and the same processing procedure was applied separately for a bottom tracking pulse. Therefore, our velocity data are not significantly affected by the ship's motions.

In order to reference the velocity profiles to a fixed geographic coordinate system we need to use the ADCP's magnetic compass. Near Barrow the relevant horizontal component of the earth's magnetic field strength vector is only 11 000 nT, which is less than half the field strength at midlatitudes. To compound compass problems, the steel hull of the icebreaker is within less than 7 m from the ADCP compass and caused significant biases in the compass readings (Münchow et al. 1995). A thorough compass calibration was thus necessary and we used all available navigational GPS and ADCP data for this purpose. The octagonal ship track (Fig. 1) consisted of eight straight sections along which the ship sailed at constant speed. During this 16 hour long "calibration run" the ADCP compass range was only 120° instead of the expected 360°. Using GPS data we first mapped the 120° range into the full 360° range before we applied a magnetic compass and a standard ADCP calibration routine (Münchow et al. 1995). The final results of the calibration routine are shown in Fig. 2, which compares the ship's absolute velocity over ground from navigational data (GPS) with that from the bottom tracking (BT) ADCP pulse. The agreement is excellent, and we claim accuracy of about 2% in speed and 3 deg in direction.

We neglect tidal currents in this study. In Barrow Canyon barotropic tidal currents are very weak, about 0.02 m s^{-1} (Mountain et al. 1976; Kowalik and Proshinsky 1995) and are thus ignored. In contrast, subtidal velocities in Barrow Canyon frequently exceed 0.5 m s^{-1} (Mountain et al. 1976; Aagaard and Roach 1990).

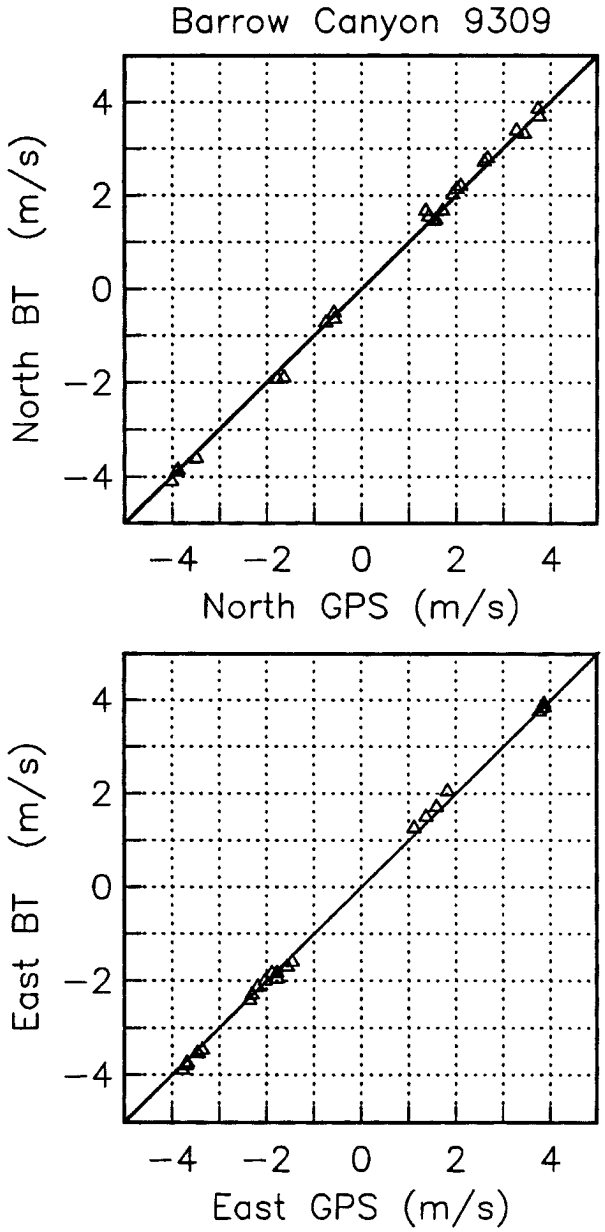

FIG. 2. Comparison of the ship's velocity determined from navigational data (GPS) and the bottom tracking (BT) of the ADCP towed besides the CCGS *Henry Larsen* on 24–25 September 1993 after extensive calibrations (after Münchow et al. 1995).

The neglected small tidal currents are similar to the velocity uncertainties that remain after the calibration.

The hydrographic surveys of the CCGS *Henry Larsen* employed a small self-contained SeaBird SEACAT CTD that includes a pump to improve the flushing characteristics of the conductivity cell. Four weeks prior to our survey in September 1993, the USCGC *Polar Star* surveyed the area to the north of Barrow Canyon in water generally deeper than 700 m using a SeaBird SBE 911 Plus system (R. Perkin 1996, personal communication). All sensors were calibrated before and after each cruise against bottle data samples that were analyzed with a Guildline salinometer. The SEACAT CTD was compared in situ against a more accurate Falmouth Scientific Inc. CTD system. The accuracy of the SEACAT and SBE 911 Plus systems are better than 0.01 psu for salinity, 0.01°C for temperature, and about 1 db for pressure data.

3. Hydrography

Satellite imagery of SSMI brightness temperatures for the summer of 1993 (not shown) indicates an ice edge more than 200 km to the north of our study area. Both the USCGC *Polar Star* and the CCGS *Henry Larsen* thus operated in ice free waters when they surveyed the velocity and density fields in the Barrow Canyon area. Four CTD casts were collected from the USCGC *Polar Star* on 18 August as part of a survey of the Canada Basin. A more extensive survey by the CCGS *Henry Larsen* resulted in 7 and 18 CTD casts that were collected on 9 September and 24–25 September, respectively. The three hydrographic surveys of Barrow Canyon span about 6 weeks and are thus not strictly synoptic. Furthermore, Aagaard and Roach (1990) showed that upcanyon upwelling events are episodic and last for only a few days. Below we will report such an event. Nevertheless, the dominant timescale of the water properties below the seasonal surface mixed layer and seaward of the canyon is much longer than 6 weeks (Carmack 1990) and thus can be interpreted as quasi-synoptic.

Figure 3 shows a composite of hydrographic data collected along an across-shelf transect that extends from the 3000-m to the 70-m isobath along the axis of the canyon based on data from three different surveys (Fig. 1). The waters of the surface mixed layer are strongly affected by ice melt, solar heating, and local wind mixing at a daily timescale, and are therefore not discussed. A shallow pycnocline about 40 m below the surface separates the surface layer and constitutes the base of the seasonal mixed layer. Below the shallow pycnocline a more weakly stratified layer of cold ($T < -1.0$°C) but relatively fresh ($S \approx 32.1$–33.1 psu) water diminishes in thickness from about 100 m offshore to less than 40 m inshore (Figs. 3b and 3c). Below a second deeper pycnocline are relatively warm ($T > 0.0$°C) and salty ($S > 34.0$ psu) waters containing mixtures of warm and salty Atlantic layer waters (Coachman and Barnes 1963). Throughout our discussion we use the term ''halocline'' exclusively for the deep pycnocline that overlies the Atlantic layer.

The halocline slopes strongly toward shore from 200 m to less than 100 m (Fig. 3). Taking the $\sigma_\theta = 27.5$ kg m^{-3} isopycnal to represent the halocline, we depict in Fig. 4 this density surface $Z_{27.5}(x, y)$ for the Beaufort Sea. In the deep Canada Basin $Z_{27.5}$ generally slopes by about 50 m over a distance L of about 200 km, that is, $\Delta Z_{27.5}/L \approx 0.25 \times 10^{-3}$. Near Barrow Canyon $Z_{27.5}$

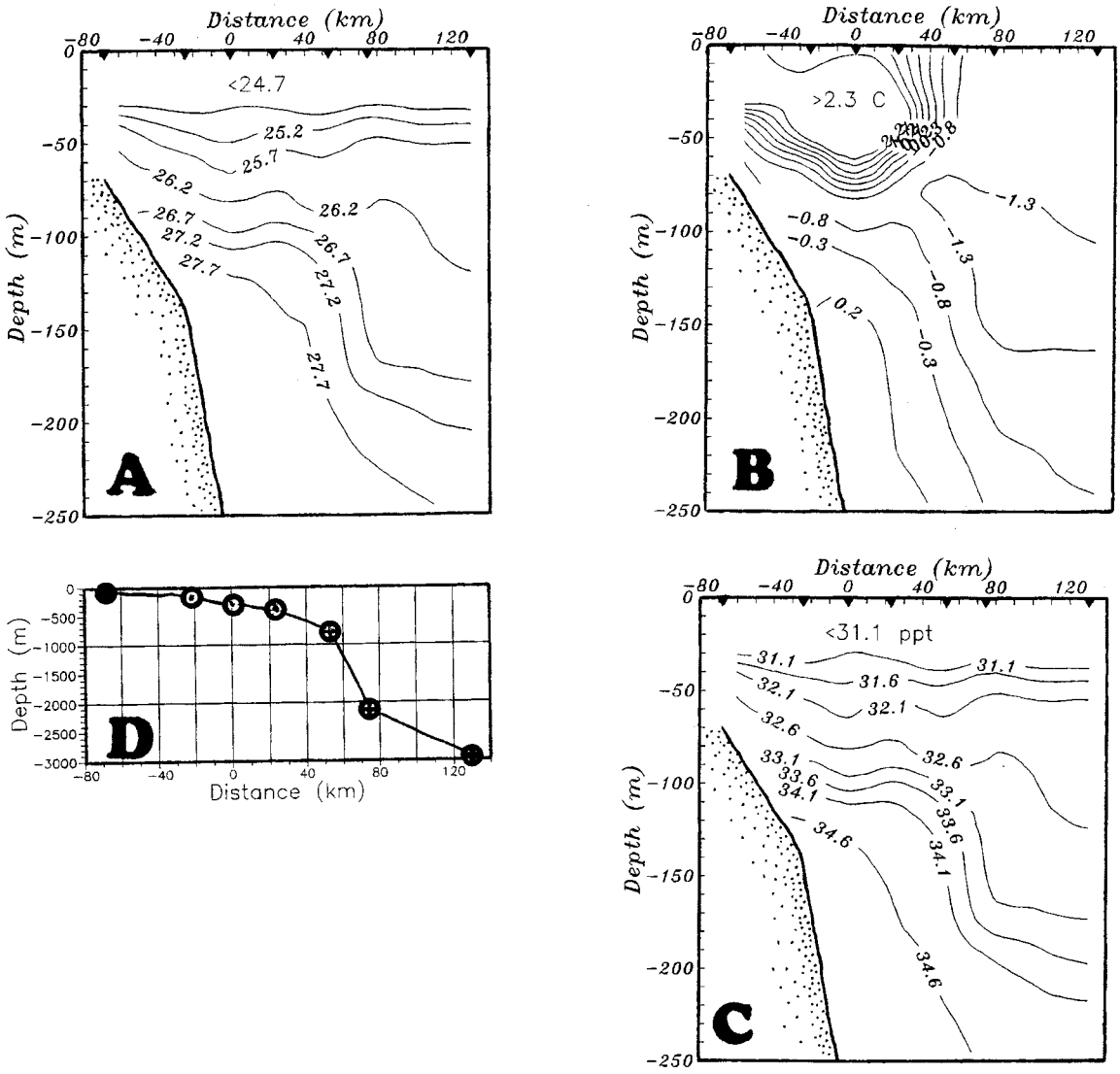

FIG. 3. Density (a), temperature (b), salinity (c), and bottom variations (d) along the axis of Barrow Canyon and across the shelf break. Symbols for station locations in Fig. 3d conform to those used in Fig. 1. Only data below the surface mixed layer at about 40 m are shown. See Fig. 1 for station locations. Note the strongly sloping deep pycnocline (σ_t = 27.2) that lies within the main halocline of the Arctic Ocean.

slopes about 100 m over a distance L of about 100 km, that is, $\Delta Z_{27.5}/L \approx 1.00 \times 10^{-3}$. The slope of the pycnocline thus increases by a factor of ~4 in the vicinity of Barrow Canyon. The dramatic rise of the halocline from about 250 m in Canada Basin to less than 100 m within Barrow Canyon represents a narrow westward flowing geostrophic current with a magnitude of about 15 cm s^{-1} relative to the 250-m depth or the bottom if the total water depth is less than 250 m deep (Fig. 5). A current roughly 100 km wide emerges over the outer continental shelf with a baroclinic transport of about 1.7 Sv. The geostrophic surface current is the well-known anticyclonic Beaufort Gyre, driven by the wind stress distribution over the Arctic Ocean.

Temperature–salinity correlations from the two CCGS *Henry Larsen* surveys show that all hydrographic data fall onto a single curve (Fig. 6). Temperature extrema of about 5°C and −l.7°C occur near salinities of 31.0 and 32.8 psu, respectively. These two water types are Bering Sea summer (Coachman and Barnes 1961) and Bering Sea winter water, respectively. The two water masses mix with each other. Furthermore, Bering Sea summer waters mix with cold and fresh surface ice melt (salinity < 29 psu), while the Bering Sea winter waters mix with warm but saline deep waters (salinity > 34 psu). The saline deep waters contain a small fraction of Atlantic waters (Coachman and Barnes 1963). We thus find four water types that form three distinct water masses.

Density, salinity, and temperature distribution across

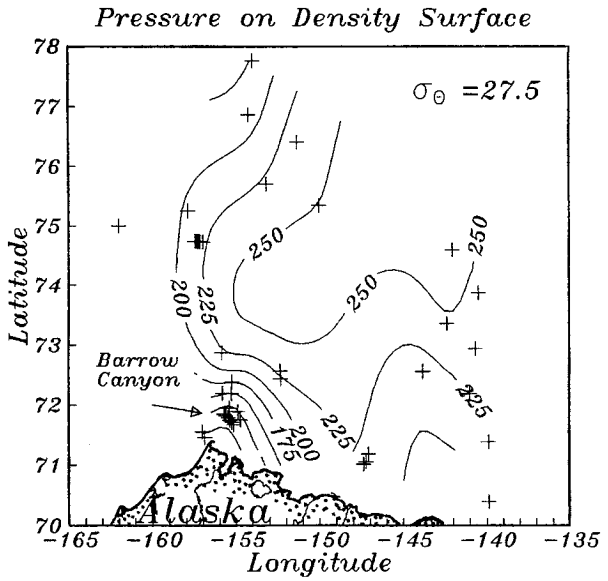

FIG. 4. Depth of the $\sigma_t = 27.5$ isopycnal throughout most of the Canadian Basin in the summer of 1993. Note the intensification of the isopycnal slope near Barrow Canyon.

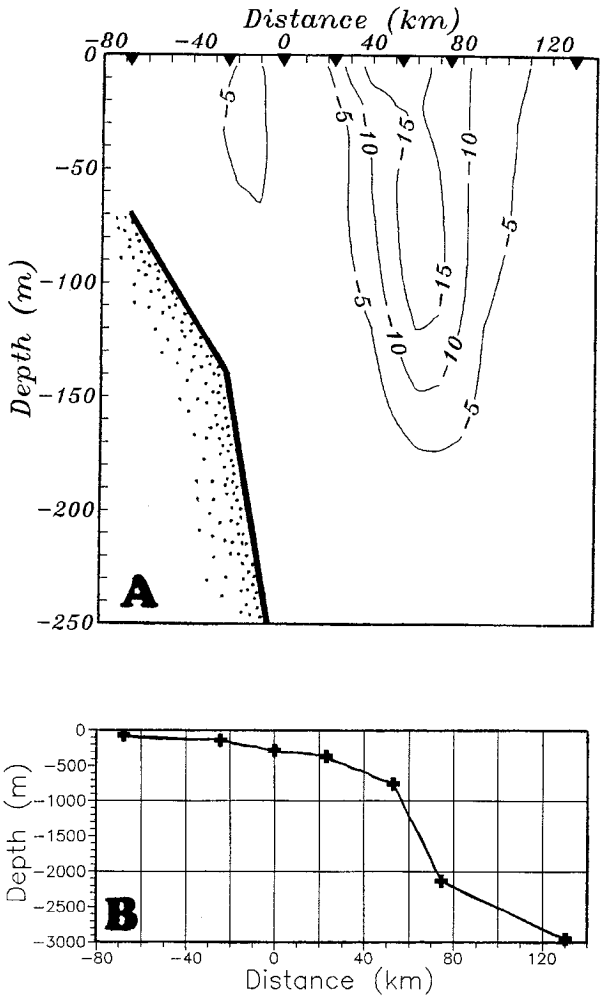

FIG. 5. Derived geostrophic velocity (a) and bottom variations (b) along the axis of Barrow Canyon and across the shelf break. See Fig. 1 for station locations and Fig. 3 for the density field from which the geostrophic shear is derived.

the canyon at the central section B (see Fig. 1 for location) describe a three-layer system. Figure 7 shows distinct pycnoclines that appear at depth about 50 m and 100 m. The deep pycnocline (or $Z_{27.5}$) slopes across the canyon by a similar amount as it slopes across the shelf break, that is, $\Delta Z_{27.5}/L \approx 0.8 \times 10^{-3}$. The sharp and sloping pycnocline at depths 100 ± 15 m separates waters of Atlantic origin from Bering Sea winter water, while the pycnocline at depths 50 ± 20 m separates Bering Sea winter from Bering Sea summer water. The upper pycnocline here appears as the core of the very warm surface waters (Fig. 7c) about 20 km from the coast; offshore waters with these properties constitute Bering Sea summer waters. The core of the warm water is also a core of strong northward flow (discussed below); that is, these waters are advected downcanyon from the south. Waters between the two pycnoclines are the coldest waters present with temperatures approaching the freezing point. Surface waters on the eastern side of the canyon are about 2°C colder than they are on the western side next to the coast. This feature indicates lateral entrainment of cold Chukchi winter shelf waters into the canyon. In our discussion of the velocity field we indeed find that the cold waters enter the canyon from the Chukchi shelf and slope, that is, the Barrow Canyon entrains cold shelf/slope waters along its western rim, which also constitutes the shelf break of the Chukchi Sea.

The density field near Barrow Canyon is strongly three-dimensional. The sloping deep isopycnals ($\sigma_\theta > 26.5$) constitute the dynamically most interesting feature as they represent the main Arctic halocline. The across-canyon tilt of the main Arctic halocline in the canyon is of the same order of magnitude as the tilt of the halocline across the continental slope. The halocline thus slopes upward into the canyon even in the absence of winds when it is raised toward the western wall of the canyon. While the cause of the alongcanyon halocline slope is unclear, the across canyon isopycnal tilt is consistent with a northward flowing current in thermal wind balance. Qualitatively each of the observed isopycnal slopes implies a thermal wind shear of about 25 cm s^{-1} to the north (canyon) and east (shelf break) relative to a level of no motion at 250 m.

4. Kinematics

Our velocity surveys of Barrow Canyon consist of five acrosscanyon sections. We label these sections A through E (Fig. 1). Section A was profiled first (9 September 1993), section B second (24 September 1993), the half circles C and D third and fourth, and section E was profiled last (25 September 1993) as a repeat of

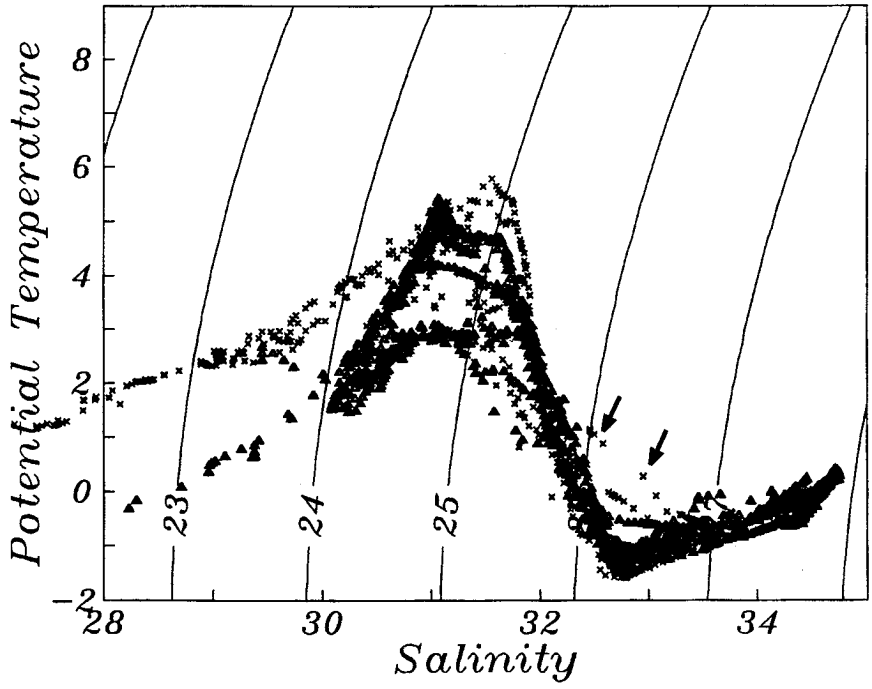

FIG. 6. Potential temperature vs salinity diagram for data collected on 9 September (×) and 24–25 September (△) of 1993 over Barrow Canyon (see Fig. 1 for station locations). Winds were locally upwelling favorable on 9 September when anomalous mixing between deep Atlantic layer and Bering Strait summer water occurs (arrows).

section B. Table 1 lists pertinent details of each section, while Fig. 8 places the surveys into a temporal context. Figure 8 marks the time of our surveys on the axis of a month-long time series of wind vectors and air temperature. The winds were generally weak and variable throughout the study period. Speeds exceed 10 m s^{-1} only on 7 and 17 September when they were upwelling favorable in the eastern Chukchi Sea and on 13 September when they were locally downwelling favorable. Air temperatures increased smoothly until 15 September when they reached 8°C. They decreased after 15 September to below the freezing point and reached −5°C during our last survey on 25 September. The large temperature difference between the air (Fig. 8b) and the water (Fig. 7) will explain the divergence in the temperature flux over Barrow Canyon, which will be discussed below.

In order to introduce the general flow field pattern, we show in Fig. 9 the depth-averaged current vectors from all surveys. The main feature is a strong northward flow that enters the canyon from the south with slightly enhanced transports near the canyon center. Maximum barotropic speeds exceed 0.5 m s^{-1}. The energetic flow passes Point Barrow, becomes laterally sheared, veers to the right, and breaks up into three parts. The trifurcation is best seen along the northern semicircle. From west to east we identify a weak northward flow directly into the Arctic Ocean along the canyon axis (B3), an anticyclonic turning along contours of bottom topography (B2), and a rapid anticyclonic turning across contours of bottom topography (B1). A weak cyclonic recirculation cell occupies most of the northwestern portion of the canyon near 72°N latitude. Note also the weaker but still sizable (10 cm s^{-1}) flow along the northern rim of the canyon. We thus observe a spatially variable barotropic flow in the lower canyon. In contrast, the barotropic flow in the upper canyon just off Barrow appears spatially uniform. This does not, however, apply to the baroclinic flow that we discuss next.

Prior to and during the first survey on 9 September 1993 the local winds in the Chukchi Sea were both strong and upwelling favorable along the western coast of Alaska. Figures 10a and 10b show the along- and acrosscanyon flow at section A. The alongcanyon component is 42° from true north (T). Alongcanyon currents across the 30-km wide section A range from 0.05 m s^{-1} on the western side of the canyon to 0.7 m s^{-1} over the 150-m deep center of the canyon. The flow on the eastern side of the canyon near the surface is 0.3 m s^{-1} and increases to 0.5 m s^{-1} at depth. Deep isopycnals, for example, $\sigma_t = 26.5$ kg m^{-3}, are raised by more than 50 m near the coast (Fig. 10c) and thus indicate strong vertical motion. Note also that the acrosscanyon flow component (Fig. 10b) away from the coast exceeds 0.2 m s^{-1} near the surface within about 20 km of the coast. If the flow field is uniform along the coast, then the

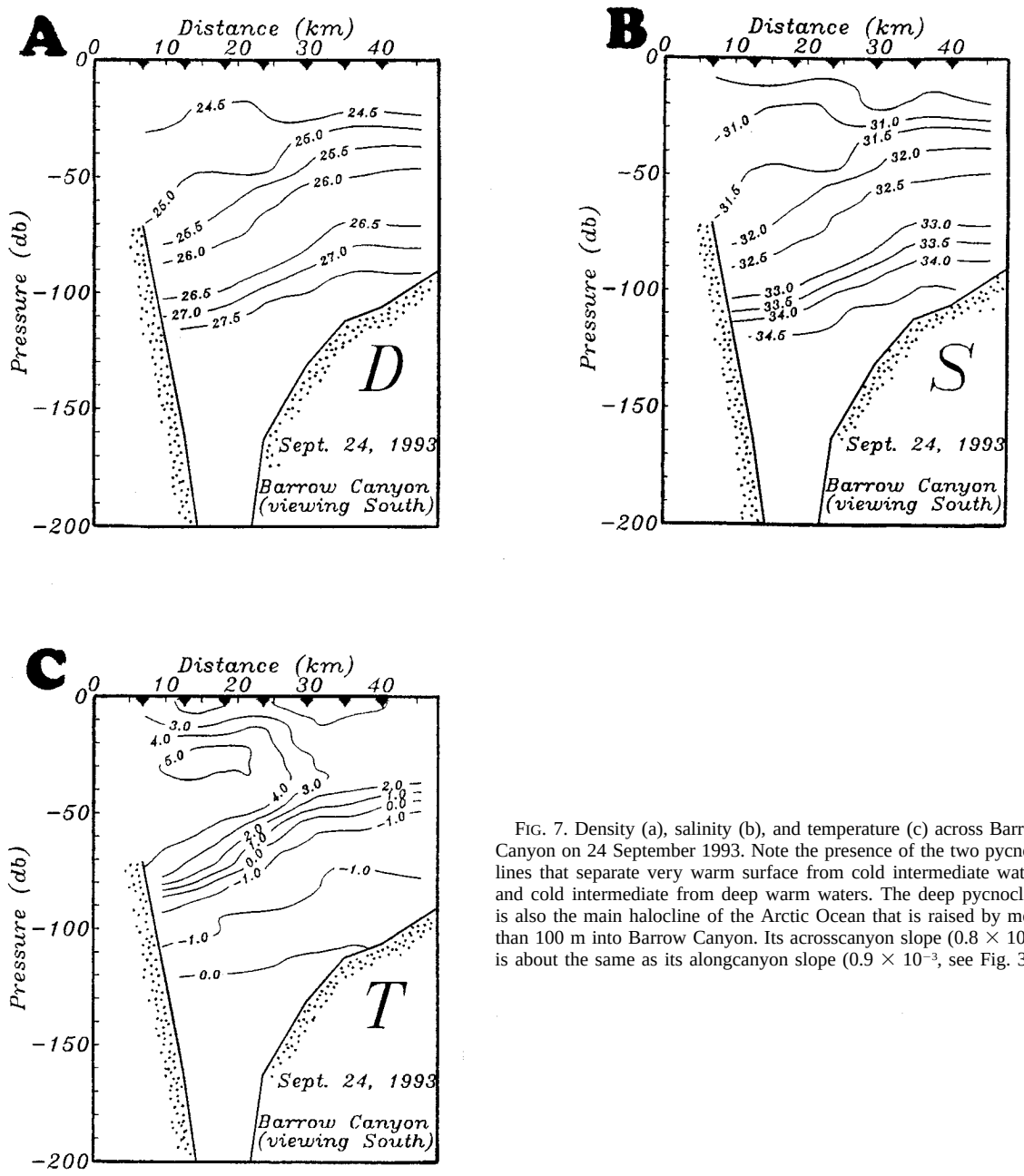

FIG. 7. Density (a), salinity (b), and temperature (c) across Barrow Canyon on 24 September 1993. Note the presence of the two pycnoclines that separate very warm surface from cold intermediate waters and cold intermediate from deep warm waters. The deep pycnocline is also the main halocline of the Arctic Ocean that is raised by more than 100 m into Barrow Canyon. Its acrosscanyon slope (0.8×10^{-3}) is about the same as its alongcanyon slope (0.9×10^{-3}, see Fig. 3).

TABLE 1. Northward transport across Barrow Canyon sections.

Section	Date (mo/d/yr)	Start–end time (UTC)	Center time (UTC)	Transport (Sv)	Notes
A	09/09/93	1903–0346	2328	0.94 ± 0.05	Upstream
B	09/24/93	1959–0145	2252	0.45 ± 0.10	Central CTD
C	09/25/93	0145–0742	0443	1.12 ± 0.11	Semicircle south
D	09/25/93	0742–1336	1140	0.97 ± 0.19	Semicircle north
E	09/25/93	1336–1641	1511	1.07 ± 0.11	Central (same as B)

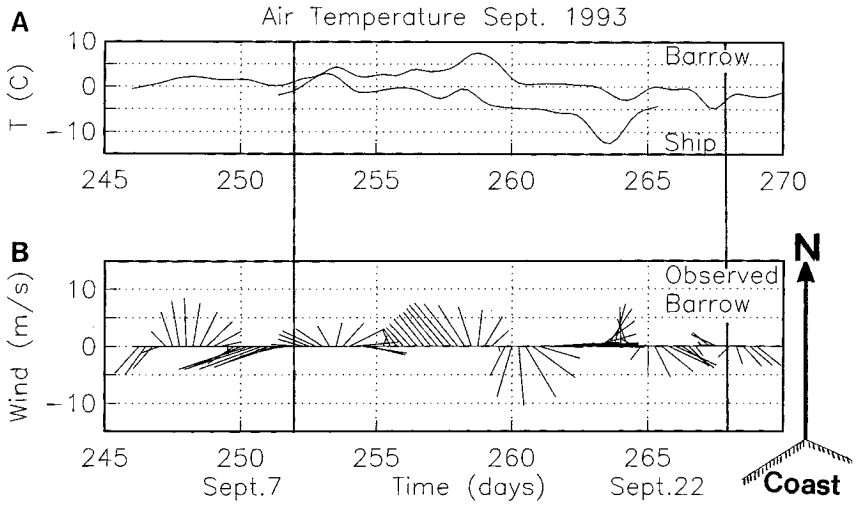

FIG. 8. Time series of (a) air temperature and (b) wind vectors at Point Barrow airport for the month of September 1993. The vertical lines on day 252 and 268 indicate the time of the two surveys by the CCGS *Henry Larsen.*

divergence due to the acrosscanyon flow results in a scale $W = (\Delta z \Delta v)/\Delta y$ for the vertical flow from

$$\nabla \cdot \mathbf{u} \approx \partial_y v + \partial_z w = 0,$$

where $\mathbf{u} = \mathbf{u}(y, z)$ is the velocity vector with components (u, v, w), while (y, z) are the acrosscanyon and vertical coordinates, respectively. In order to estimate a vertical velocity scale W, we approximate $\partial_y v \approx \Delta v/\Delta y$ and $\partial_z w \approx W/\Delta z$, take $\Delta v = 0.2$ m s^{-1}, $\Delta y = 20$ km, and $\Delta z = 20$ m from Fig. 9b, and obtain $W = 2 \times 10^{-4}$ m s^{-1} $\approx$ 17 m day^{-1}. While this scale is large, it is not unreasonable. It suggests that sustained locally upwelling favorable winds from the northeast can ventilate lower halocline waters by raising them toward the surface where they mix with Bering Sea waters. We indeed observe such mixing in the temperature–salinity correla-

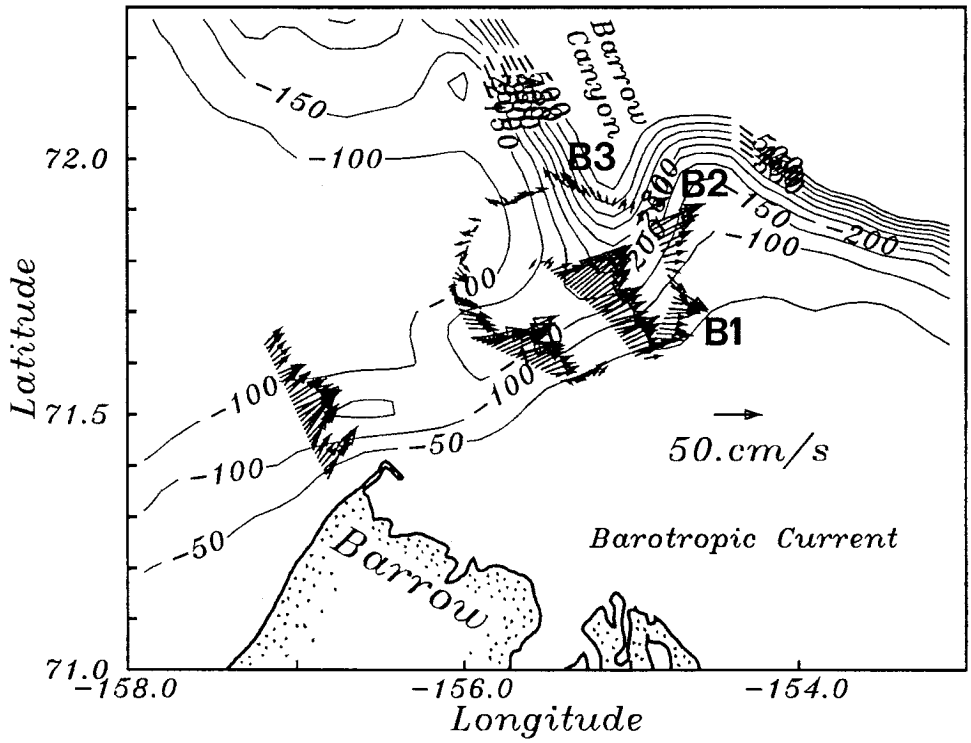

FIG. 9. Map of depth-averaged velocity vectors over Barrow Canyon.

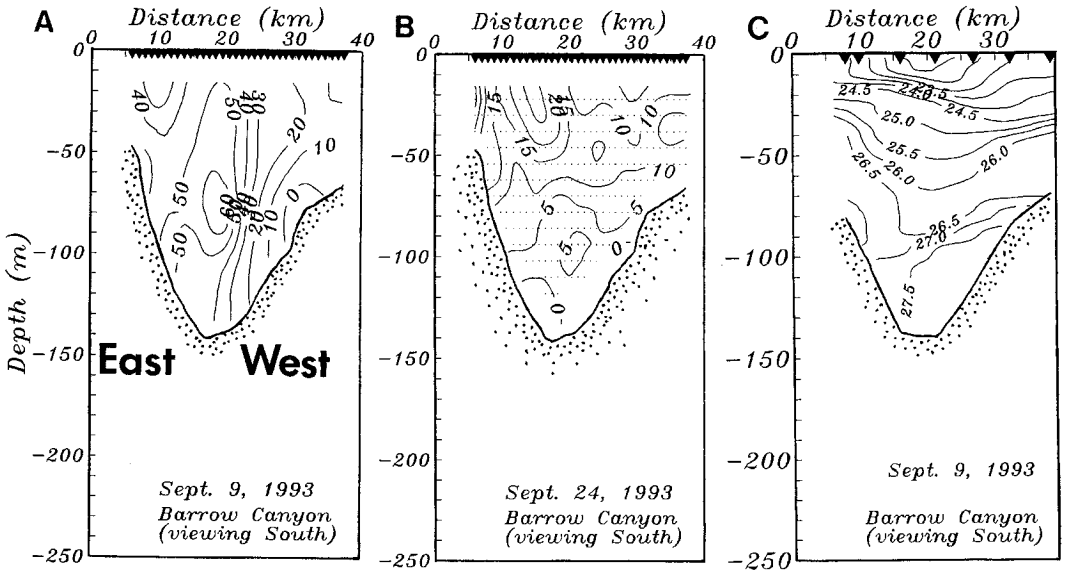

FIG. 10. Velocity and density across upper Barrow Canyon on 9 September 1993: (a) velocity component along 42 deg T, positive is northward (alongcanyon); (b) velocity component along 132 deg T, positive is eastward (acrosscanyon); (c) density.

tion of Fig. 6. On several stations Bering Sea summer waters mix with salty ($S > 33.2$ psu) warmer waters. This mixture thus erodes the T_{min} layer near 32.8 psu.

We surveyed the 40-km wide Barrow Canyon area more extensively on 24–25 September and completed four sections across the canyon about 50 km to the north of Barrow within a day. Winds during this second survey were moderate (5 m s^{-1}) from the northeast. Winds 5 days prior to the survey were also weak (<5 m s^{-1}) but variable. The flow is thus affected little by local winds.

Two sections B and E sample the same transect at two different times about 16 hours apart. Figures 11a and 11b depict the alongcanyon flow across these sections. We find an intense northward outflow with velocity magnitudes exceeding 0.7 m s^{-1} near the surface (Fig. 11b). The flow below the main halocline is weak (<0.1 m s^{-1}) during the first survey (Fig. 11a); however, it becomes surprisingly strong (>0.5 m s^{-1}) during the second survey (Fig. 11b). Above this intense deep outflow, we find at a depth of 80 m a 50-m thick and 10-km wide core of much reduced velocities (>0.3 m s^{-1}) next to the coast. While the spatial structure of the flow ap-

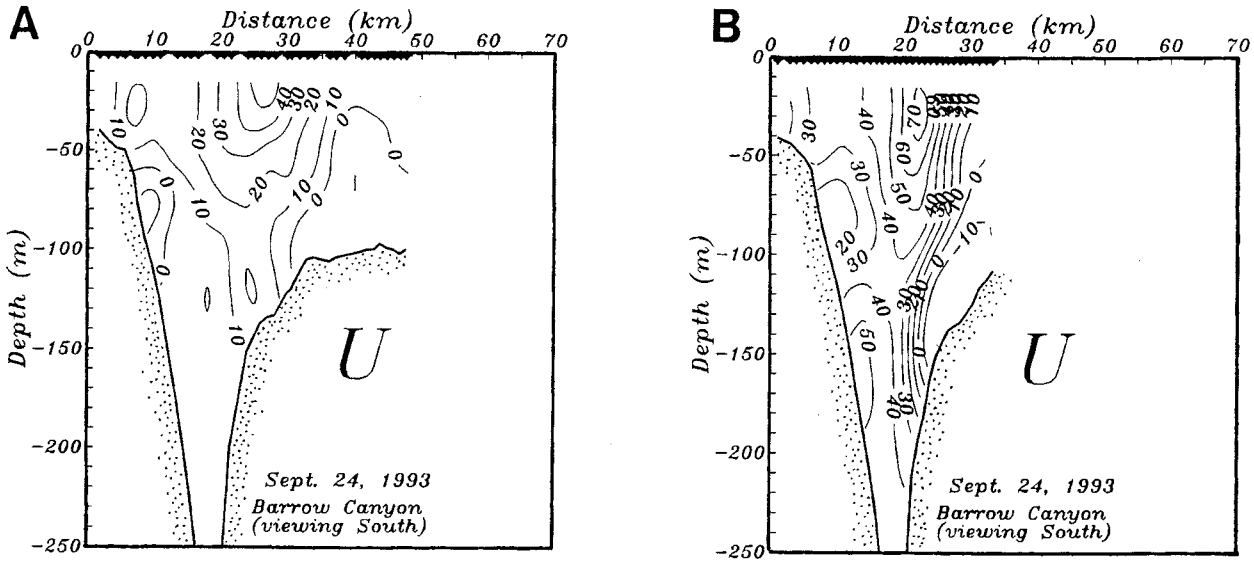

FIG. 11. Alongcanyon velocity across the lower Barrow Canyon: (a) section B, center time 2252 UTC 24 September 1993 and (b) section E, center time 1511 UTC 25 September 1993.

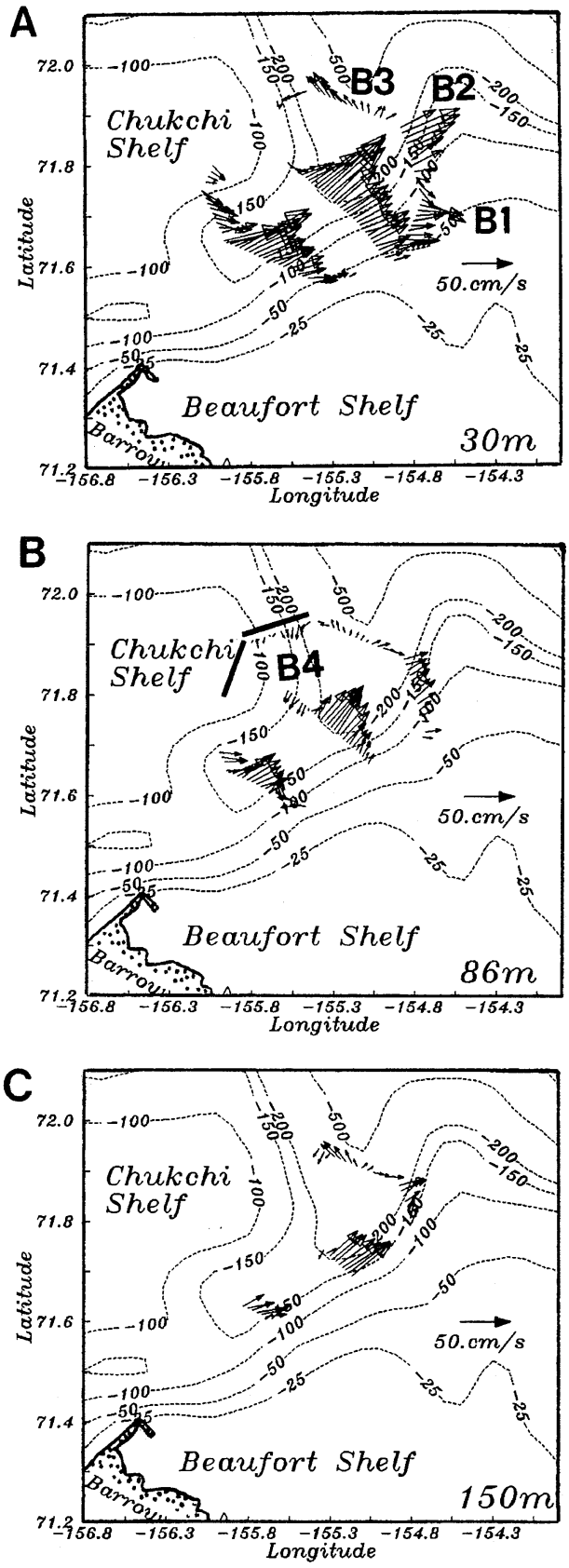

pears similar (e.g., surface-intensified northward outflow near the canyon axis, bottom-intensified inflow near the Chukchi shelf, and a pocket of reduced flow next to the coast), the magnitude of the flow increases by almost a factor of 2 within an inertial period (12.7 h). Unfortunately, we do not have CTD data for the repeat of the section and thus do not know how the density field adjusts to the rapidly changing flow field.

The increase of the northward flow adjacent to the Alaska coast occurs concurrently with an increase of the southward inflow on the opposite side of the canyon. The enhanced inflow of about 0.15 m s^{-1} at depth (120 m) lies adjacent to the outflow of about 0.7 m s^{-1} near the surface (30 m). The lateral shear of the alongcanyon flow appears to be uniform with depth near this shear zone, which is only 5 km wide. Currents vary by about 0.4–0.5 m s^{-1} over this distance and the lateral shear is about $+0.6f$, where f is the Coriolis parameter. The magnitude of the lateral shear has important implications with respect to the momentum and vorticity balances of the flow as it represents a Rossby number for a unidirectional channel flow.

We next describe the along- and acrosscanyon distribution of current vectors at different depths in order to quantify the baroclinicity of the observed flow. Figure 12a shows a map of current vectors measured at a depth of 30 m. Speeds here exceed 0.7 m s^{-1} near the center of the canyon and extend at least 50 km along the canyon. The surface flow is thus spatially coherent and represents the terminus of the Alaska Coastal Current (Bourke and Paquette 1976). Near the shelf break, however, this current breaks into three different branches, all of which have a northward flow component. The first branch, B1, turns anticyclonically onto the Beaufort shelf east of Point Barrow. The radius of curvature of the flow is small, about 25 km; however, this scale does not enter the dynamics since both the inertial length scale U/f and the internal deformation radius ND/f are about 2–5 times smaller. Here U ($\sim$0.5 m s^{-1}) is a velocity scale, f ($\sim 1.4 \times 10^{-4}$ s^{-1}) is the local Coriolis parameter, D ($\sim$50 m) is the vertical scale of the horizontal motion, and $N = (g\partial_z\rho/\rho_0)^{1/2}$ ($\sim$0.02 s^{-1}) is the buoyancy frequency with the vertical density gradient $\partial_z\rho$ ($\sim$0.04 kg m^{-4}), a reference density ρ_0 ($\sim$1027 km m^{-3}) and, g (=9.81 m s^{-2}) the gravitational constant (Gill 1982). The second branch, B2, turns anticyclonically also; however, it does so with a larger radius of curvature of about 100 km, which appears to correspond the length scale of the curving bathymetry. Here we trace the velocity maximum at the 30-m depth of all three acrosscanyon sections to determine this scale.

←

FIG. 12. Maps of velocity vectors at (a) 30 m, (b) 86 m, and (c) 150 m below the surface from ADCP survey of sections C, D, and E on 24–25 September 1993. The labels B1, B2, B3, and B4 indicate different branches of currents near Barrow Canyon.

Branch B2 supplies the slope current of the Beaufort Sea with relatively fresh and warm waters. Aagaard (1984) calls the eastward extension of this topographically steered slope current the Beaufort Undercurrent. The third branch, B3, constitutes a much reduced flow down the axis of the canyon into the deep Arctic Ocean where it becomes entrained into the wind-driven Beaufort gyre.

The waters at middepth (86 m) follow a similar pattern but with only two instead of three branches (Fig. 12b). Branch B1 disappears as it is a shallow surface feature only; that is, the strong anticyclonic flow across the eastern canyon slope onto the Beaufort Shelf seen at a depth of 30 m (Fig. 12a) is not present at 86 m (Fig. 12b). At 86-m depth we discover a flow into the canyon along its western boundary (labeled B4 in Fig. 12b). A 0.15 m s^{-1} strong flow enters the canyon along the 150-m isobath from the Chukchi shelf in the northwest, follows this isobath, and turns southward into the canyon. The upcanyon flow component over the western canyon causes the deflection of the downcanyon flow at the southernmost section. Chukchi shelf/slope waters thus become entrained into the northward flow and recirculate within the canyon. It is this flow that supplies the layer of cold water that insulates halocline waters from buoyant surface waters.

It is not clear, however, that this upcanyon flow originates from the Chukchi slope as discussed above. Another interpretation of the flow is suggested by Fig. 13, which shows data from a velocity section 40 km long across the Chukchi slope. The section consists of adjacent legs from the two semicircles C and D (see Fig. 1 for locations). The velocity component normal to this section is about 20° T; that is, negative velocities are into the canyon as viewed to the west. Figure 13 reveals that the inflow into the canyon from the Chukchi slope may be part of a baroclinic anticyclonic ''eddy.'' Two velocity cores with flows in opposite directions are visible at a distance of 25 and 32 km and a depth of about 50 and 60 m, respectively. The height of the eddy is about 50 m as velocities reduce to zero near the surface and bottom. The western rim of Barrow Canyon thus constitutes another possible generation site for the abundant eddies that populate the Canada Basin.

Currents at a depth of 150 m are generally northward out of the canyon (Fig. 12c). The weak upcanyon flow, B4, along the western canyon wall persists. Along the central section E, however, northward velocities at the 150-m depth approach 0.4 m s^{-1}. A substantial portion of the northward flow is barotropic at section E at this point in time.

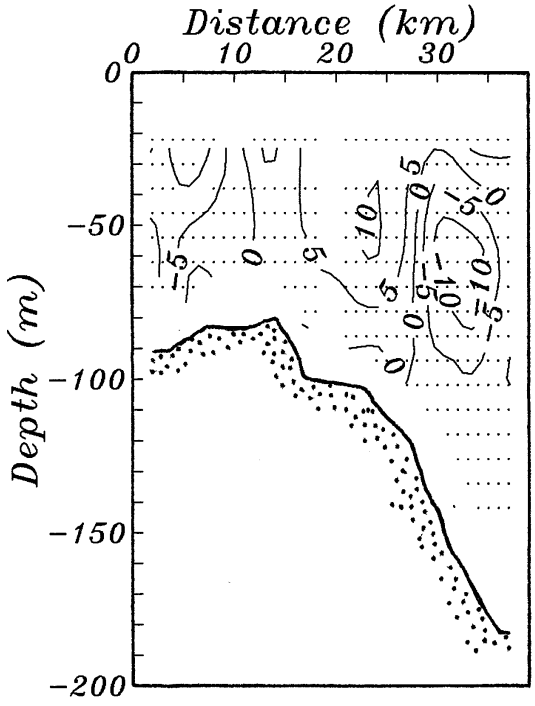

FIG. 13. Alongshelf currents to the northwest of Barrow Canyon showing a possible baroclinic anticyclonic eddy over the continental slope. Figure 12b shows the location of this composite section.

5. Fluxes

Here we combine velocity and hydrographic observations in order to estimate property fluxes through Barrow Canyon. These estimates are potentially sensitive to the details of the interpolation and integration methods used. This is especially true since the ADCP does not measure currents within about 20 m of the surface and about 10–30 m off the bottom. All across-section integrations are thus performed on gridded data; that is, the irregular spaced data are first interpolated onto a regular grid. Grid scales are 2 m in the vertical and 2 km in the horizontal. We use the method of minimum curvature, which is mathematically equivalent to a biharmonic spline interpolation (McIntosh 1990). Evaluating the sensitivity of the method, we estimate all fluxes both without and with the top 20 m of the water column and present our results in Tables 2 and 3, respectively.

a. Volume

The volume flux across each section is computed as the integral of the normal component of the velocity transport vectors (Fig. 12 and Table 1). Transports are all to the north and vary in magnitude from 0.5 ± 0.10 to 1.1 ± 0.11 Sv (Sv ≡ 10^6 m^3 s^{-1}). The uncertainty is due a uniform error of 0.02 m s^{-1}. If the data are both synoptic and error free, then the conservation of mass requires that the net flow through a closed volume be exactly zero. The transports across the two semicircles C and D are 1.12 ± 0.11 Sv into and 0.97 ± 0.19 Sv out of the closed volume, respectively (Table 1). Our measurements along this closed control volume thus balance mass to within a measurement error of 0.15 ± 0.15 Sv. We note, however, that the transports of the repeat sections B and E differ by a factor of

TABLE 2. Northward fluxes across Barrow Canyon sections (below 20 m).

Section	Date, time (mo/d/yr, UTC)	Volume flux (10^6 m^3 s^{-1})	Temperature flux (10^{12} W)	Salt flux (kg m^3 s^{-1})	Buoyancy flux (10^4 m^4 s^{-3})
A	09/09/93, 2328	0.94 ± 0.05	2.8 ± 0.8	31 ± 2	1.2 ± 0.2
B	09/24/93, 2252	0.45 ± 0.10	4.4 ± 0.6	14 ± 3	0.8 ± 0.2
C	09/25/93, 0443	1.12 ± 0.11	6.4 ± 0.8	36 ± 4	1.8 ± 0.3
D	09/25/93, 1140	0.97 ± 0.19	5.1 ± 0.8	32 ± 7	1.2 ± 0.3
C–D		0.15 ± 0.15	1.3 ± 0.8	4 ± 6	0.6 ± 0.3

2. The time between the successive profiling was about 16 h (Table 1) or about 1.3 inertial cycles; the repeat sections B and E thus are not entirely synoptic as the flow field varies at the inertial-time scale. In contrast, the data along the two semicircle sections C and D are only 6 hours apart and thus are at least quasi-synoptic.

As our observations indicate a balance of mass, we can estimate a barotropic transport streamfunction ψ from our data. Modifying the approach of Cheng et al. (1992), we integrate the depth-averaged normal component of the velocity vector $\mathbf{U}\cdot\mathbf{n}$ along the ship track in small increments ds; that is,

$$\psi(s) = \int \mathbf{U}\cdot\mathbf{n}\, ds,$$

where $s = s(x, y)$, and (x, y) are longitude and latitude. The integration is started arbitrarily at $s_0(x_0, y_0)$, with a value of $\psi_0 = 0$ and $x_0 = 155.4°$W and $y_0 = 71.7°$N. Figure 14 shows contours of ψ in units of Sverdups using data from transects C, D, and E (see Table 1). The streamlines indicate an upstream jet bounded by the 100-m isobath in the narrow upper part of the canyon. The jet separates from the eastern canyon wall as the canyon widens, exhibits a weak meander, and closely follows contours of f/H. Here f is the (constant) Coriolis parameter (planetary vorticity) and H is the local water depth. Potential vorticity $(f + \xi)/H$ thus may be conserved along streamlines as the relative vorticity $\xi = \partial_x v - \partial_y u$ is always smaller than $0.4f$ and changes little along streamlines. We speculate that the topographic slope stabilizes the flow, a hypothesis that needs to be verified by a separate analytical study. The streamlines also indicate some recirculation in the northwestern part of the wide canyon as fluid enters from the Chukchi shelf, crosses the western topographic slope of the canyon, turns cyclonically, and leaves the canyon on a path along the canyon axis.

During our survey the total volume transport through Barrow Canyon exceeds 1.0 Sv. For comparison, the annual mean transport through Bering Strait more than 500 km to the south is 0.8 ± 0.2 Sv. Instantaneous transports reach 2 Sv during the ice-free summer season and correlate strongly with atmospheric pressure gradients and slightly less with the local winds (Coachman and Aagaard 1988). In order to relate our transport observations to those through Bering Strait more clearly, we need to analyze the property fluxes through Barrow Canyon for each water mass separately. Using Fig. 7 as a guide, we define three layers by their respective densities that roughly represent the Bering Sea summer, Bering Sea winter, and Atlantic waters. These water masses are bounded by two pycnoclines, whose center we define by the $\sigma_t = 25.5$ kg m^{-3} and the $\sigma_t = 27.0$ kg m^{-3} isopycnals. For section B we show in Fig. 15 the thickness, the center depth, the layer-averaged alongcanyon velocity, and the volume transport per unit width as a function of acrosscanyon position for each of the three layers. The integral of the transport across the section gives the total volume transport. These are 0.29, 0.10, and 0.09 Sv for the Bering Sea summer, Bering Sea winter, and Atlantic waters, respectively. Thus, 60% of the total transport is contained in the surface layer with waters lighter than 1025.5 kg m^{-3}. The surface layer reduces in thickness across the canyon from about 60 m near the coast of Alaska to less than 20 m on the Chukchi shelf. Most of the water column, however, is occupied by Bering Sea winter and Atlantic waters, which contribute about 40% to the total transport. We then conclude that 60% of the downcanyon transport consists of Bering Sea summer waters, while the remainder consists in roughly equal portions of entrained Bering Sea winter and previously upwelled Atlantic waters.

b. Heat

Advection of warm Bering Sea summer water represents a heat flux toward the Arctic Ocean. Paquette

TABLE 3. Northward fluxes across Barrow Canyon sections (extrapolated to the surface).

Section	Date, time (mo/d/yr, UTC)	Volume flux (10^6 m^3 s^{-1})	Temperature flux (10^{12} W)	Salt flux (kg m^3 s^{-1})	Buoyancy flux (10^4 m^4 s^{-3})
A	09/09/93, 2328	1.15 ± 0.06	5.0 ± 0.5	37 ± 2	2.1 ± 0.2
B	09/24/93, 2252	0.63 ± 0.12	6.3 ± 0.8	20 ± 4	1.4 ± 0.2
C	09/25/93, 0443	1.34 ± 0.13	7.5 ± 0.9	43 ± 4	2.2 ± 0.3
D	09/25/93, 1140	1.20 ± 0.22	7.3 ± 1.0	39 ± 7	1.9 ± 0.4
C–D		0.14 ± 0.18	0.2 ± 1.0	4 ± 6	0.3 ± 0.4

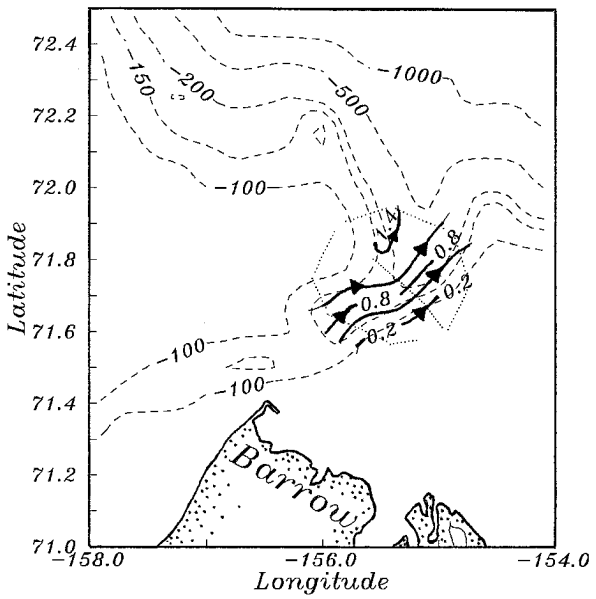

FIG. 14. Transport streamfunction in Sv from ADCP observations along the shiptrack indicated by the dotted line. The dashed lines represent the 100-m, 150-m, 200-m, 500-m, and 1000-m isobaths.

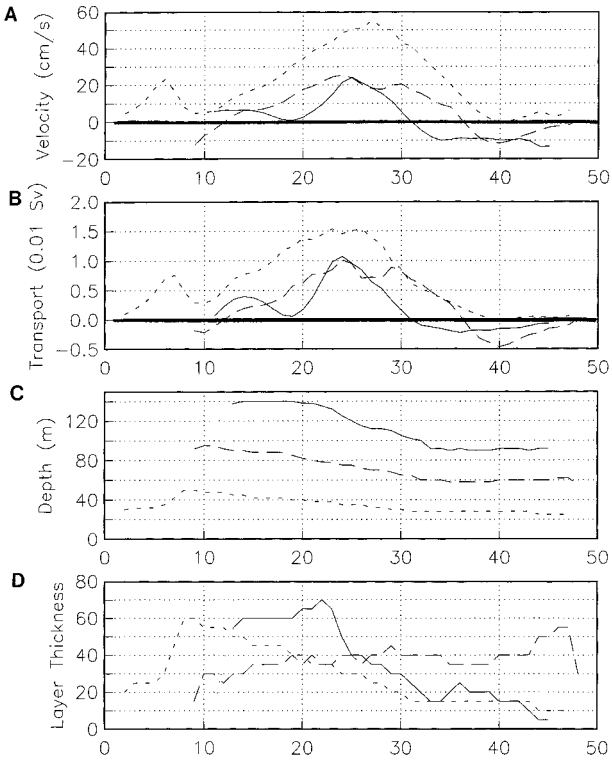

FIG. 15. Acrosscanyon profiles of (a) velocity, (b) transport, (c) depth, and (d) thickness of each of three layers. Layers 1 (short dash), 2 (long dash), and 3 (solid line) are defined by $\sigma_t < 1025.5$ kg m^{-3}, $1027.0 > \sigma_t > 1025.5$ kg m^{-3}, and $\sigma_t > 1027.0$ kg m^{-3}, respectively.

and Bourke (1981) postulate that much of the heat transported north melts ice along its path and thus causes an enhanced retreat of the ice edge. We combine our velocity and temperature data to quantify the advective fluxes through Barrow Canyon. The advective temperature flux F_h is generally defined as

$$F_h \equiv \int\int f_h \, dz \, dy,$$

where f_h is the temperature flux per unit area; that is,

$$f_h = \rho_0 C_p(\theta - \theta_0)V,$$

and $V(x, y, z)$ is the velocity component normal to a section (y, z), $\theta(x, y, z)$ is the potential temperature in degrees Celsius, $\theta_0 = 0.0$°C is a reference temperature, $\rho_0 = 1026$ kg m^{-3} is the density of sea water, and $C_p = 3986$ J kg^{-1} K^{-1} is the specific heat capacity of sea water at constant pressure. Generally, the temperature flux F_h depends upon the reference temperature θ_0. It represents a meaningful measure of the heat flux if and only if the mass flux across a section equals zero (Montgomery 1974). In the following we distinguish between a temperature flux that depends upon a reference temperature and a heat flux that does not. Sections C and D form a closed volume with a zero mass flux to within measurement error. The sum of the temperature fluxes through these two sections thus constitutes a meaningful measure of the absolute heat flux to the atmosphere.

Figures 16a, 16b, and 16c show the resulting temperature fluxes per unit area f_h across sections B, C, and D, respectively. Not surprisingly, the fluxes are concentrated near the surface about 30 km from the coast where f_h reaches between 6×10^6 W m^{-2} and 8×10^6 W m^{-2}. The uncertainty of the temperature flux due to a current of 0.5 ± 0.02 m s^{-1} and a temperature of 4 ± 0.01°C is about 0.5×10^6 W m^{-2}. The advective temperature fluxes per unit area are thus significantly different from zero only within about 60 m of the surface, which consists dominantly of Bering Sea summer water. Note, however, that the core of the temperature fluxes ($f_h > 4 \times 10^6$ W m^{-2}) is only 10 km wide and changes little along the canyon from section to section. The splitting of the northward flow into three different branches also shows in the temperature fluxes for the northernmost section D (Fig. 16c). Evaluating the integral F_h over the entire cross-sectional area, we arrive at temperature fluxes of about $4.4 \pm 0.6 \times 10^{12}$ W, $6.4 \pm 0.8 \times 10^{12}$ W, and $5.1 \pm 0.8 \times 10^{12}$ W for sections B, C, and D, respectively. They are listed in Table 2 along with corresponding fluxes of volume, buoyancy, and salt. The heat flux across the volume enclosed by sections C and D is the difference between the temperature fluxes across the southern section C and the northern section D that form the closed volume. This difference is about $1.3 \pm 0.8 \times 10^{12}$ W, which is the amount of heat lost through the surface that encloses the volume. Here we assume that all heat is lost through the surface to the atmosphere. The volume enclosed by sections C and D has a surface area of about 2×10^9

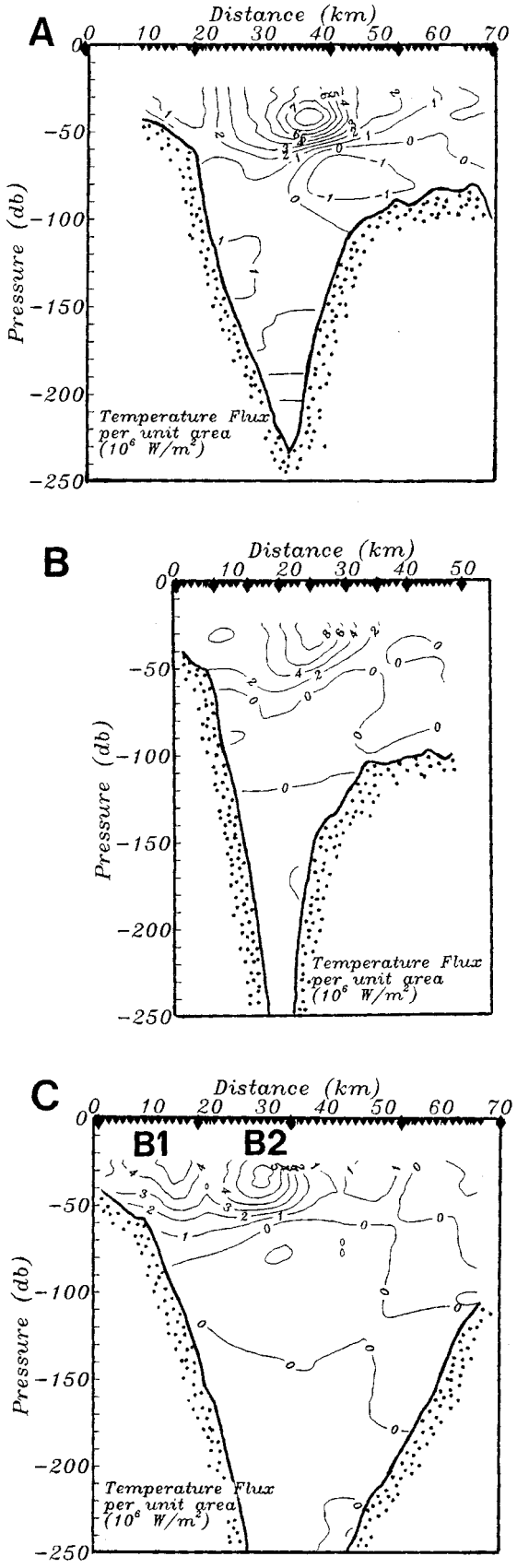

m^2, which results in a net surface heat loss of about 650 $\pm$ 400 W m^{-2}. As we do not have any direct velocity observations within about 20 m of the surface, this heat is lost to a surface layer about 20 m deep. If we extrapolate our velocity measurements linearly to the surface, then we arrive at the flux estimates shown in Table 3. None of the flux estimates are now significantly different from zero as the errors generally exceed the net flux estimates. Flux estimates are so rare, however, that even order of magnitude estimates may prove useful to design future experiments. Extrapolating our velocity measurements to the surface we arrive at a net heat flux of 120 $\pm$ 490 W m^{-2} from the ocean to the atmosphere. This estimate is similar to estimates of the surface heat flux Q of a warm ocean below a cold atmosphere from bulk formulas such as

$$Q = \rho_{\text{air}} C_p C_H U_{\text{wind}} (T_{\text{ocean}} - T_{\text{sea}})$$

(Gill 1982), where ρ_{air} ($\sim$1.2 kg m^{-3}) is the density of air; C_p ($\sim$3986 J kg^{-1} K^{-1}) is the specific heat capacity; C_H ($\sim$0.0011) is a Stanton number; U_{wind} ($\sim$5 m s^{-1}) is the wind speed; T_{air} (~ -6°C) is the air temperature; and T_{ocean} ($\sim$4°C) is the ocean temperature. With these values for our survey we arrive at a vertical heat flux $Q \sim 260$ W m^{-2}. The turbulent atmospheric bottom boundary layer will thus be deeper near Barrow Canyon than beyond. The oceanic heat transport to the atmosphere at the seasonal transition from summer to winter near Barrow Canyon rivals that of major current systems such as the Gulf Stream, which supplies about 350 W m^{-2} to the atmosphere (Isemer and Hasse 1987).

c. Buoyancy

The Bering Sea summer waters that discharge into the Arctic Ocean through Barrow Canyon are both warm and fresh relative to Arctic surface waters. The flow of these light waters northward thus represents a flux of positive buoyancy into the Arctic Ocean. Lateral buoyancy forces are often balanced by the Coriolis force through the thermal wind relation. Large buoyancy fluxes through Barrow Canyon thus constitute a point source of baroclinic forcing. The steady transport of positively buoyant Bering Sea summer waters through Barrow Canyon into the Arctic Ocean acts dynamically similar to a river that discharges light water onto a sloping continental shelf from an estuary that is wide relative to the internal deformation radius. We define the advective buoyancy flux as

←

FIG. 16. Northward temperature transport per unit width across sections (a) B (central), (b) C (southern semicircle), and (c) D (northern semicircle). See Fig. 1 for locations. Units are watts per square meter; both the contour interval and the uncertainty of an individual estimate are 1 W m^{-2}. The labels B1 and B2 in (c) indicate the two branches of the anticyclonically turning flow.

$$F_b \equiv \int \int f_b \, dz \, dy,$$

where f_b is the buoyancy flux per unit area; that is,

$$f_b = (\rho_0 - \rho) g V / \rho_0,$$

where $V(x, y, z)$ is the velocity component normal to a section (y, z), $g = 9.81$ m s^{-2} is the gravitational constant, ρ(x, y, z) is the in situ density of sea water, and $\rho_0 = 1027.6$ kg m^{-3} is a reference density of sea water. The latter represents upper halocline water (Fig. 3). The procedure to estimate the buoyancy flux is similar to that employed for the heat flux and is thus not repeated here. The buoyancy flux through Barrow Canyon contributes about $0.6 \pm 0.3 \times 10^4$ m^4 s^{-3} of buoyancy to the Arctic Ocean (Table 2). By comparison, the Delaware estuary off the eastern seaboard of the United States releases about 10^2 m^4 s^{-3} of buoyancy into the Atlantic Ocean where it forces a 0.1 m s^{-1} strong buoyancy-driven coastal current whose alongshore velocity is in thermal wind balance (Münchow and Garvine 1993). We therefore hypothesize that the large buoyancy flux through Barrow Canyon contributes to the dynamics of the Beaufort Undercurrent.

6. Conclusions

Barrow Canyon is a conduit of mass, heat, and momentum at the intersection of the broad Chukchi shelf, the narrow Beaufort shelf, and the deep Arctic Ocean. The location, geometry, and complex forcing fields all result in a delicately arranged three-dimensional flow and density field. A strongly sheared jet transports between 0.5 and 1.1 Sv toward the north. During our daylong survey the volume transport changed by a factor of 2, demonstrating that the flow through Barrow Canyon is strongly time dependent. We hypothesize that our spatial velocity observations captured the last stage of a large flow reversal after an upcanyon surge brought both Arctic halocline and Atlantic layer waters onto the shelf through Barrow Canyon. Nevertheless, about 60% of the northward volume flux consists of warm and fresh Alaskan coastal waters that entered the Chukchi shelf in the summer from the Bering Sea more than 500 km to the south. The remaining 40% are Bering Sea winter shelf and Atlantic layer waters. The latter must have been upwelled onto the shelf prior to our survey, possibly through the canyon itself (Bourke and Paquette 1976).

The depth of the main halocline (defined here by the $\sigma_t = 27.5$ kg m^{-3}) in Canada Basin is about 250 m. Within Barrow Canyon it reaches depths less than 100 m. Inside the canyon the alongcanyon isopycnal slope is tilted across the canyon as well, and the density field is thus strongly three-dimensional. During strong local upwelling favorable winds the halocline within the canyon adjacent to the Alaska coast is raised by about 17 m day^{-1}. One such event occurred on 9 September 1993 when we observed a mixing event between upper halocline and surface waters. In the absence of such winds the halocline tilts across the canyon in the thermal wind sense due to a northward surface flow; that is, it slopes upward toward the Chukchi Sea.

Near Barrow Canyon the warm waters in the upper sections of the canyon coincide with a jet 10–20 km wide with northward velocities that exceed 0.7 m s^{-1}. Largest alongcanyon flows occur over the deepest part of the canyon while the flow contacts both canyon walls. As the canyon widens to the north, however, the northward jet separates from the Chukchi shelf. Farther downstream the coastline changes orientation by about 90 deg, and the single jet disintegrates into at least three branches. A portion of the surface flow immediately moves across the eastern canyon wall onto the Beaufort shelf.

Despite the large surface flow across the canyon wall (branch B1, see Fig. 12a) we do not observe clear manifestation of eddy generation as suggested by D'Asaro (1988b). According to this theory a frictional torque near Point Barrow would reduce the relative vorticity of the flow through Barrow Canyon to values smaller than f. Anticyclonic eddies should form about once or twice every day; here we had hoped to witness such eddy formation. While we do observe a strong alongcanyon flow, its largest horizontal current shear is $+0.6f$, which is of the wrong sign (cyclonic), at the wrong location (away from the coast), and a factor 2 too small. Horizontal current shears within about 5 km of the coast are anticyclonic but their magnitude is less than $0.2f$ and thus too small to support the generation mechanism proposed by D'Asaro (1988b).

Most of the northward transport follows bottom contours and may conserve potential vorticity. The bottom topography bends eastward more smoothly than does the coastline; that is, flow separation probably does not take place here. Instead, the gently turning flow may follow the topography and contribute to the Beaufort Undercurrent. We also find evidence of recirculation within the canyon as a small fraction of the northward mass transport flows down the canyon axis toward the Arctic Ocean, while on the opposing (or western) side of the canyon we find a southward upcanyon flow of about 0.15 m s^{-1}. Closer inspection of this inflow reveals that the waters entering the canyon from the north originate from the continental slope of the Chukchi Sea to the northwest of Barrow Canyon.

Our observations represent a single snapshot of a temporally and spatially variable flow field. Despite both temporal and spatial variability of the fields, a few general patterns emerge, such as upwelling of Atlantic waters from below the main Arctic halocline. Furthermore, Barrow Canyon, which is about three internal deformation radii wide, accommodates opposing baroclinic flows on either side, has a zone of much enhanced lateral current shears that reach $0.6f$, and supports the formation of both cyclonic and anticyclonic eddies along its rim.

It is not clear, however, whether the flows are geostrophically controlled even though the observed vertical current shears agree qualitatively with thermal wind shears. Using a three-dimensional regional circulation model of the study area, Signorini et al. (1997) find that while the vertical velocity shear correlates strongly with the baroclinic pressure gradient in the thermal wind sense, the across-canyon momentum balance is ageostrophic. Secondary flows result from a local imbalance of the Coriolis acceleration and the baroclinic pressure gradients. It is also not clear if the flow is baroclinically or barotropically unstable, even though the model suggests that the canyon flow is stable.

In order to answer these questions and to understand the dynamics of the flow near the shelf break off Barrow we need to conduct both observational and numerical process studies. It is at this location that Pacific and Atlantic waters interact most vigorously and that topographically induced upwelling ventilates the main Arctic halocline in summer in conjunction with wind-induced local upwelling. The generation and dynamics of vortices near Barrow Canyon, too, will remain unclear and speculative without further observations. Observational studies should consist of a small array of moored upward looking ADCPs to profile the entire water column.

Acknowledgments. The senior author (AM) conducted the field work as a postdoctoral fellow at Scripps Institution of Oceanography (SIO). There Nancy Bray gave unselfish advice, encouragement, and support; Jennifer Davis overcame the many bureaucratic hurdles; Clinton Winant generously gave the ADCP tow; Charly Coughran and Myrl Henderschott taught AM to use and repair the instrument in the field. Aboard the CCGS *Henry Larsen,* Captain Gomes and his crew performed innovatively in a scientific mode of operation. Rob Macdonald of the Institute of Ocean Sciences, Canada, was a generous chief scientist and responsible deck hand during the last night of the 6-week-long expedition. Rick Pearson and Douglas Sieberg of IOS, Canada, confidently assembled ADCP, tow, and cables at sea. Charly Coughran of SIO and Dyrl Simons of RDI provided technical and moral support back in San Diego. Finally, Tom Curtin of the Office of Naval Research sponsored this work and insured the ADCP system against its loss at sea. The work was funded by ONR through Grants N00014-94-0041 and N00014-93-0093 to Rutgers University and SIO, respectively.

REFERENCES

Aagaard, K., 1984: The Beaufort undercurrent. *The Alaskan Beaufort Sea,* P. W. Barnes and Coeditors, Academic Press, 47–71.

——, 1989: A synthesis of the Arctic Ocean circulation. *Rapp. P.-V. Reun. Cons. Int. Explor. Mer,* **188,** 11–22.

——, and A. T. Roach, 1990: Arctic ocean–shelf exchange: Measurements in Barrow Canyon. *J. Geophys. Res.,* **95,** 18 163–18 175.

——, and E. C. Carmack, 1994: The Arctic Ocean and climate: A perspective. *The Polar Oceans and Their Role in Shaping the Global Environment,* O. M. Johannessen and Coeditors, Amer. Geophys. Union, 5–20.

——, L. K. Coachman, and E. C. Carmack, 1981: On the halocline of the Arctic Ocean. *Deep-Sea Res.,* **28,** 529–545.

Ahlnäs, K., and G. R. Garrison, 1984: Satellite and oceanographic observations of the warm coastal current in the Chukchi Sea. *Arctic,* **37,** 244–254.

Bourke, R. H., and R. G. Paquette, 1976: Atlantic water on the Chukchi shelf. *Geophys. Res. Lett.,* **3,** 629–632.

Candela, J., R. C. Beardsley, and R. Limeburner, 1992: Separation of tidal and subtidal currents in ship-mounted acoustic Doppler current profiler observations. *J. Geophys. Res.,* **97,** 769–788.

Carmack, E. C., 1990: Large scale physical oceanography of polar oceans. *In Polar Oceanography, Part A: Physical Sciences,* W. O. Smith, Ed., Academic Press, 171–222.

Cheng, C., R. C. Beardsley, and R. Limeburner, 1992: The structure of the Kuroshio southwest of Kyushu: Velocity, transport and potential vorticity fields. *Deep-Sea Res.,* **39,** 245–268.

Chereskin, T. K., M. D. Levine, A. J. Harding, and L. A. Regier, 1989: Observations of near-inertial waves in acoustic Doppler current profiler measurements made during the mixed layer dynamics experiment. *J. Geophys. Res.,* **94,** 8135–8145.

Coachman, L. K., and C. A. Barnes, 1961: The contribution of Bering Sea water to the Arctic Ocean. *Arctic,* **14,** 147–161.

——, and ——, 1963: The movement of Atlantic water in the Arctic Ocean. *Arctic,* **16,** 9–16.

——, and K. Aagaard, 1988: Transports through Bering Strait: Annual and inter-annual variability. *J. Geophys. Res.,* **93,** 15 535–15 539.

D'Asaro, E. A., 1988a: Observations of small eddies in the Beaufort Sea. *J. Geophys. Res.,* **93,** 6669–6684.

——, 1988b: Generation of submesoscale vortices: A new mechanism. *J. Geophys. Res.,* **93,** 6685–6693.

Gawarkiewicz, G., and A. J. Plueddeman, 1995: Topographic control of thermohaline structure in the Barents Sea polar front on the south flank of Spitsbergen Bank. *J. Geophys. Res.,* **100,** 4509–4524.

Geyer, W. R., and R. Signell, 1990: Measurements of tidal flow around a headland with a shipboard acoustic Doppler current profiler. *J. Geophys. Res.,* **95,** 3189–3197.

Gill, A. E., 1982: *Atmosphere–Ocean Dynamics.* Academic Press, 662 pp.

Hanzlick, D., and K. Aagaard, 1980: Freshwater and Atlantic water in the Kara Sea. *J. Geophys. Res.,* **85,** 4937–4942.

Hart, J. E., and P. D. Killworth, 1976: On open ocean baroclinic instability in the Arctic. *Deep-Sea Res.,* **23,** 637–645.

Hufford, G. L., 1973: Warm water advection in the southern Beaufort Sea August–September 1971. *J. Geophys. Res.,* **78,** 2702–2707.

——, 1974: On apparent upwelling in the southern Beaufort Sea. *J. Geophys. Res.,* **79,** 1305–1306.

Huthnance, J. M., 1992: Extensive slope currents and the ocean shelf boundary. *Progress in Oceanography,* Vol. 29, Pergamon Press, 161–196.

Isemer, H.-J., and Z. Hasse, 1987: *The Bunker Climate Atlas of the North Atlantic Ocean.* Vol. 2: *Air–Sea Interaction,* Springer-Verlag, 252 pp.

Johnson, M., and H. J. Niebauer, 1995: The 1992 summer circulation in the Northeast Water Polynya from acoustic Doppler current profiler measurements. *J. Geophys. Res.,* **100,** 4301–4307.

Klinck, J. M., 1989: Geostrophic adjustment over submarine canyons. *J. Geophys. Res.,* **94,** 6133–6144.

Klinger, B. A., 1994: Baroclinic eddy generation at a sharp corner in a rotating system. *J. Geophys. Res.,* **99,** 12 515–12 531.

Kowalik, Z., and A. Y. Proshutinsky, 1994: The Arctic Ocean tides. *The Polar Oceans and Their Role in Shaping the Global Environment,* O. M. Johannessen and Coeditors, Amer. Geophys. Union, 137–158.

Manley, T. O., and K. Huskins, 1985: Mesoscale eddies in the Arctic Ocean. *J. Geophys. Res.,* **90,** 4911–4930.
McIntosh, P. C., 1990: Oceanographic data interpolation: Objective analysis and splines. *J. Geophys. Res.,* **95,** 13 529–13 541.
Montgomery, R., 1974: Comments on ''Seasonal variability of the Florida Current'' by Niiler and Richardson. *J. Mar. Res.,* **32,** 533–534.
Mountain, D. G., L. K. Coachman, and K. Aagaard, 1976: On the flow through Barrow Canyon. *J. Phys. Oceanogr.,* **6,** 461–470.
Münchow, A., and R. W. Garvine, 1993: Buoyancy and wind forcing of a coastal current. *J. Mar. Res.,* **51,** 293–322.
——, ——, and T. F. Pfeiffer, 1992: Subtidal currents from a shipboard Acoustic Doppler Current Profiler in tidally dominated waters. *Contin. Shelf Res.,* **12,** 499–515.
——, C. S. Coughran, M. C. Hendershott, and C. D. Winant, 1995: Performance and calibration of a subsurface towed acoustic Doppler current profiler. *J. Atmos. Oceanic Technol.,* **12,** 435–444.
New, A. L., 1992: Factors affecting the quality of shipboard acoustic Doppler current profiler data. *Deep-Sea Res.,* **39,** 1985–1992.
Newton, J. L., K. Aagaard, and L. K. Coachman, 1974: Baroclinic eddies in the Arctic Ocean. *Deep-Sea Res.,* **21,** 707–719.
Overland, J. E., and A. T. Roach, 1987: Northward flow in the Bering and Chukchi seas. *J. Geophys. Res.,* **92,** 7097–7105.
Paquette, R. G., and R. H. Bourke, 1974: Observations on the coastal current of Arctic Alaska. *J. Mar. Res.,* **32,** 195–207.
——, and ——, 1981: Ocean circulation and fronts as related to ice melt-back in the Chukchi Sea. *J. Geophys. Res.,* **86,** 4215–4230.
Pollard, R. T., and L. A. Regier, 1992: Vorticity and vertical circulation at an ocean front. *J. Phys. Oceanogr.,* **22,** 609–625.
Signorini, S. R., A. Münchow, and D. Haidvogel, 1997: Flow dynamics of a wide Arctic canyon. *J. Geophys. Res.,* in press.
Stern, M. E., and J. A. Whitehead, 1990: Separation of a boundary jet in a rotating fluid. *J. Fluid Mech.,* **217,** 41–69.
Stigebrandt, A., 1984: The North Pacific: A global scale estuary. *J. Phys. Oceanogr.,* **14,** 464–470.